
VaViM and VaVAM: Autonomous Driving through Video Generative Modeling

Florent Bartoccioni[†] Elias Ramzi[†] Victor Besnier Shashanka Venkataramanan
 Tuan-Hung Vu Yihong Xu Loick Chambon¹ Spyros Gidaris Serkan Odabas
 David Hurych Renaud Marlet² Alexandre Boulch Mickael Chen* Éloi Zablocki
 Andrei Bursuc Eduardo Valle Matthieu Cord¹

valeo.ai, Paris, France

Project page: <https://valeoai.github.io/vavim-vavam/>

Abstract

We explore the potential of large-scale generative video models for autonomous driving, introducing an open-source auto-regressive video model (VaViM) and its companion video-action model (VaVAM) to investigate how video pre-training transfers to real-world driving. VaViM is a simple auto-regressive video model that predicts frames using spatio-temporal token sequences. We show that it captures the semantics and dynamics of driving scenes. VaVAM, the video-action model, leverages the learned representations of VaViM to generate driving trajectories through imitation learning. Together, the models form a complete perception-to-action pipeline. We evaluate our models in open- and closed-loop driving scenarios, revealing that video-based pre-training holds promise for autonomous driving. Key insights include the semantic richness of the learned representations, the benefits of scaling for video synthesis, and the complex relationship between model size, data, and safety metrics in closed-loop evaluations. We release code and model weights at github.com/valeoai/VideoActionModel.

1 Introduction

Large-scale generative models have shattered the status quo of video generation with photorealistic, temporally coherent, high-fidelity videos synthesized from textual prompts. While generalist models such as Sora, Veo-2 [89] and VideoJAM [17] demonstrate those capabilities at large, specialist models such as GAIA-1 [44] and VISTA [31] showcase impressive performance in predicting future frames of driving videos. Generating plausible future frames suggests that those models capture meaningful representations of the world, but the exact nature of such representations, as well as any practical utility they might have for actual driving, remain open questions. To what extent do those representations encode driving-relevant features, such as scene dynamics, geometry, and semantics? How far do they apply to actual autonomous systems, enhancing downstream tasks, such as motion planning?

[†] Corresponding authors; {florent.bartoccioni, elias.ramzi}@valeo.com

* Work done while at valeo.ai, now at H company.

¹ valeo.ai & Sorbonne Université, Paris, France

² valeo.ai & ENPC, Paris, France

To answer those questions, we introduce an open-source, large-scale autoregressive video model (VaViM) and its companion video-action model (VaVAM). At the core of our approach, VaViM learns to predict future frames by modeling the joint distribution of spatio-temporal token sequences, capturing the underlying dynamics of driving scenes into dense representations. We use an image tokenizer to compress visual information into discrete tokens, providing a compact representation of each video frame. To bridge the gap between video understanding and action generation, we train an action expert module on VaViM’s learned video representation, forming our complete VaVAM system. We train that module with imitation learning to generate future driving trajectories guided by high-level goals and temporal context extracted from VaViM. That architecture forms a complete perception-to-action pipeline, enabling effective motion planning and decision-making in autonomous vehicles.

Our work is the first large-scale study to explore how video generative pre-training transfers to driving capabilities. We evaluate our approach using both open- and closed-loop driving scenarios. Our findings suggest that video-based pre-training holds great promise for autonomous driving, with the following insights:

1. The learned representations from video pre-training contain rich and meaningful semantic information.
2. Larger models generally improve video synthesis quality, reinforcing the benefits of scale for generative modeling. However, larger video models perform worse than smaller ones on semantic segmentation tasks, suggesting that better generative quality does not directly translate to better semantic understanding.
3. Scaling up the model improves performances in open-loop evaluations, and increasing training data yields further improvements. Nonetheless, scaling model size or data does not consistently improve safety metrics in closed-loop evaluations. This reveals a fundamental conflict between trajectory-following and adaptive decision-making.

Our key contributions are as follows:

- We provide data mix, scaling laws, training recipes, and a detailed reproducible protocol for training an autoregressive Video Model (VaViM) on large-scale 1800+ hours diverse driving data.
- We present a procedure to adapt a video model into a video-action model (VaVAM) using imitation learning for end-to-end driving from camera input.
- We propose new evaluations for the learned VaViM representations to assess their semantic content. Additionally, we benchmark VaVAM in both open- and closed-loop driving scenarios, emphasizing safety-critical situations. VaVAM achieves state-of-the-art performance in frontal driving scenarios on NeuroNCAP [59].

Table 1 reports all VaViM and VaVAM models produced in this research, coming in different sizes. We release both the source code and the weights for those models.

2 Related work

2.1 Video generative model

Today’s sophisticated architectures for video generation have significantly evolved since the days of Generative Adversarial Networks (GANs) [33, 76, 85]. Beyond basic generation capabilities, recent advances have focused on improving visual quality and enabling precise control over generated content. That dual evolution is visible in key developments in video data representation and video generation aligned to conditioning signals.

Continuous Representations: These methods work with real-valued embeddings in a continuous latent space, often operating on a pre-trained Variational Autoencoder (VAE) [52, 39] to compress the image or video signal spatially and reduce computation. Most modern approaches in this category build on either Diffusion or Flow Matching models. Diffusion Models (DM) [40, 75] learns to model the data distribution through a denoising process, effectively capturing the data distribution of images.

Table 1: Overview of the released models, covering different model sizes (up to 1.2B), trained on increasing amounts of data, and two model types (video generation and action learning).

MODEL	PARAMETERS (M)	OPENDV [96] <i>1700+ hours</i>	NUPLAN [13] <i>94 hours</i>	NUSCENES [12] <i>5.5 hours</i>
Pre-trained video models				
VaViM-S	185	✓		
VaViM-B	318	✓		
VaViM-L	1,200	✓		
Fine-tuned video models				
VaViM-S	185	✓	✓	✓
VaViM-B	318	✓	✓	✓
VaViM-L	1,200	✓	✓	✓
Video-action models trained with imitation learning				
VaVAM-S	185 + 21		✓	✓
VaVAM-B	318 + 38		✓	✓
VaVAM-L	1,200 + 150		✓	✓

Methods such as Video Diffusion Model (VDM) [41], Make-A-Video [80], or Align Your Latents [9] extends image diffusion model to video generation. Flow Matching [57] is similar to DM in learning continuous probability flows but contrasts with the latter by directly modeling the noise-to-image vector field. Notable works such as MovieGen [68] or pyramid flow matching [49] adapt Flow Matching to generate videos efficiently.

Discrete Representations: These approaches typically map video data into sequences of discrete tokens using vector quantization techniques (e.g., VQ-VAE [88], FSQ [62], LFQ [99] etc.). Inspired by language models, auto-regressive methods generate tokens sequentially, conditioning each token on the previous ones. Building upon the success of auto-regressive image generation [20, 72, 29], notable extensions to video generation include VideoGPT [94] and HARP [77] where the generation becomes spatio-temporal. In contrast to purely sequential prediction, Masked Image Modeling [16] uses a mask-and-predict strategy that iteratively predicts/reconstructs the missing tokens, inspired by BERT-like [26] training schemes. Models such as MagViT [98] and its improvement MagViT-v2 [99] have effectively extended such framework to video generation, while Phenaki [90] has used it to enable long video generation from text prompts.

Action-Controlled Video Generation: Integrating action-based control marks a significant advance in video generation, promising to move beyond passive generation to planning and decision-making. That direction is exemplified by modern ‘neural game engines’ [6], such as Genie [11], DIAMOND [1], or GameNGen [87], which generate, from input actions, the evolution of complex, dynamic, and tridimensional game environments. In the automotive context, state-of-the-art approaches build from driving videos towards ‘neural world simulators’ or so-called ‘world-models’ by leveraging pre-trained diffusion networks, as VISTA [31], GEM [36], and InfinityDrive [35] do, or by exploiting discrete-based auto-regressive models, as GAIA-1 [44] and DrivingWorld [46] do. However, a significant gap remains between generating realistic videos and learning representations suitable for robust decision-making. That limitation appears in current evaluation methods, which primarily use metrics that assess the visual quality [86, 102] but provide limited insight into the performance of end tasks.

2.2 Scalable Vision-based Action Learning

Traditional approaches to vision-based action learning have relied heavily on expensive human annotations such as semantic segmentation masks, bounding boxes, and step-by-step action labels to represent the scene [43, 47]. Those annotations are costly to acquire and often imperfect, creating fundamental scaling limitations: for instance, the autonomous driving dataset nuScenes [12] required over 100,000 manual object annotations. Such a bottleneck has motivated research to develop more scalable frameworks.

Vision-action models are scalable when they leverage large quantities of data without requiring proportional human effort. That typically involves learning from raw demonstrations without frame-by-frame labels (e.g., only recording human actions) or utilizing self-supervised objectives that forgo manual annotation. A seminal example is Video PreTraining (VPT) [4], which learns directly to act from unlabeled video demonstrations of gameplay, scaling to over 70,000 hours of data that would be prohibitively expensive to annotate manually.

An alternative is weak supervision at scale by leveraging internet data. Vision-Language Models (VLMs) like CLIP [69] and SigLIP [101] learn robust visual representations from readily available image-text pairs, eliminating the need for costly pixel-wise semantic annotations. Recent works such as LLaVA [58] or PaliGemma [7] follow that framework by building on top of pre-trained LLMs, resulting in vision encoders with strong semantic understanding. Building on that foundation, Vision-Language-Action (VLA) Models like RT-2 [105], OpenVLA [51] or π^0 [8] demonstrate how web-scale knowledge can be transferred to action generation in a robotic context.

In autonomous driving, the shift towards scalability is particularly evident. Early end-to-end approaches like TransFuser [21] or MILE [43] required extensive annotation to learn visual representations (e.g., HD maps, bounding boxes of agents, Bird’s-eye-view or camera semantic masks). Methods such as LMDrive [79], GPT-DRIVER [61], LLM-driver [19] or Language-MPC [78] leverage pre-trained LLMs, but they all expect to know the position of all agents in the scene at train or inference time. That implicitly assumes a perfect upstream perception stack, which is often unrealistic. Newer methods, instead, leverage VLMs to operate directly on the raw visual from expert demonstrations. For instance, DriveGPT4 [93] uses a pre-trained CLIP [69] encoder and a LLaMA-2 [84] LLM to interpret driving scenes without requiring dense semantic labels. CarLLaVA [74] further demonstrates how foundation models (LLaVA [58] and LLaMA [83]) enables closed-loop driving from raw sensor data and sparse navigational inputs.

2.3 Evaluation

Video generation: The rapid progress in large-scale generative models enabled the creation of visually compelling and temporally consistent videos [10, 89, 17, 31, 44, 36]. Those advancements suggest that generative models can capture meaningful representations of the world, potentially serving as ‘world models’ that simulate and understand physical interactions. Current practices in evaluating generative video models as world models predominantly rely on metrics such as the Fréchet Inception Distance (FID) [38] and its temporal extension, the Fréchet Video Distance (FVD) [86]. Those metrics, however, focus on perceptual quality rather than task-specific performance. In addition, they measure the similarity between generated and actual video distributions, assuming they were Gaussian, resulting in very coarse estimations of generative capabilities. They fall short, for example, in evaluating the model’s understanding of physical laws and real-world dynamics necessary for effective world simulation [104]. To address those limitations, new benchmarks such as Physics-IQ [63] or PhyWorld [50] test models’ comprehension of physical principles, including fluid dynamics and solid mechanics. Those evaluations reveal that despite achieving visual realism, models often lack the understanding to accurately predict physical interactions, highlighting a significant gap in their ability to function as reliable world simulators.

Open-loop driving: Open-loop evaluation assesses a system’s performance by comparing its predicted future trajectories against pre-recorded expert driving behavior. While that method enables evaluation with realistic traffic data without simulation, it has key limitations: most critically, it fails to measure performance in the actual deployment distribution, which comprises ‘reasonable’ trajectories that deviate from the expert’s [22, 24]. Such limitation is further highlighted in AD-MLP [100], which demonstrates that a simple MLP model taking only ego-motion as input may achieve comparable or better open-loop scores than complex perception-based methods. Furthermore, the distance between predicted and recorded trajectories is not an ideal metric in multi-modal scenarios; for instance, when merging into a turning lane, both immediate and delayed merging could be valid options, but open-loop evaluation penalizes the option not observed in the data [100]. To address those limitations, some metrics propose to cover more comprehensive aspects such as traffic violations, progress, and driving comfort [24], but the correlation between open-loop performance and actual driving performance remains loose [24].

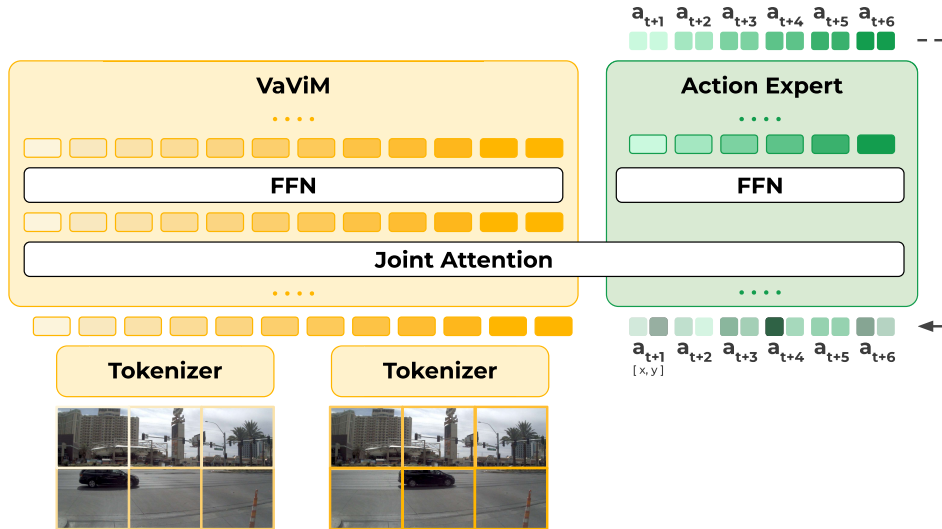


Figure 1: **End-to-end pipeline of VaVAM.** From a context of up to 8 frames, first VaViM (in yellow) builds a spatio-temporal representation, and then VaVAM’s action expert (in green) estimates the dynamic profile of the driving actions to undertake, as a trajectory of 6 waypoints sampled at 2 Hz.

Closed-loop driving: Closed-loop driving evaluation addresses the key limitations of open-loop testing by enabling model decisions to influence subsequent observations. Existing approaches can be categorized based on their simulation capabilities and trade-offs. Bird’s-eye-view-only simulators [34, 13] focus on trajectory planning but cannot evaluate end-to-end perception-based systems. Meanwhile, synthetic simulators such as CARLA [28] enable comprehensive end-to-end evaluation with dynamic agents, but their synthetic nature introduces significant domain gaps when transferring to real-world scenarios [18]. Vista [2, 3] attempts to bridge this gap through view reprojection from actual data but cannot simulate dynamic agent interactions. NavSim [25] introduces a non-reactive paradigm where agents commit to actions based on initial real-world sensor input and continue the simulation in BEV. That limits long-horizon evaluation as the system does not receive environmental feedback. Conversely, NeuroNCAP [59] currently represents the most complete solution by enabling closed-loop evaluation with dynamic agents and continuous sensory feedback through neural rendering, thus allowing for long-horizon scenarios while maintaining photorealism from real-world data.

3 Models

Our video-action model VaVAM is composed of VaViM — a self-supervised video model that learns semantic driving features through next-token prediction (Section 3.1) — and an action expert module (Section 3.2) that enables end-to-end autonomous driving from video inputs. Figure 1 illustrates that perception-to-action pipeline.

3.1 VaViM = Auto-regressive Video-Model on tokenized video stream

At its core, the auto-regressive video model captures the underlying dynamics of driving scenes by modeling the joint distribution of spatio-temporal token sequences. It operates on discrete video tokens, i.e., compact representations of video frames obtained through an image tokenizer (Section 3.1.1). By learning to predict the next token in these sequences (Section 3.1.2), VaViM builds a rich understanding of the temporal patterns in driving environments.

3.1.1 Image Tokenizer

The architecture starts by transforming continuous image data into a discrete sequence of tokens using vector quantization, a process known as visual tokenization [88], by mapping local image features to their nearest neighbors in a learned codebook. The codebook acts as a compressed visual vocabulary, enabling efficient auto-regressive modeling while preserving the essence of the visual information for downstream tasks.

More formally, consider a video clip with T frames, with each frame $X_t \in \mathbb{R}^{h \times w \times c}$ for $t \in \{1, \dots, T\}$. Here, $h \times w$ is the spatial resolution, and c is the number of channels. The encoder $f_\theta : X \rightarrow e$ processes each frame independently to produce a latent embedding $e \in \mathbb{R}^{h' \times w' \times d}$. For a given frame embedding e , at each spatial location $(i, j) \in h' \times w'$, we quantize $e^{(i,j)}$ to a discrete token $q^{(i,j)}$ by performing a nearest-neighbor lookup in the codebook $\{e_k\}$:

$$q^{(i,j)} := \arg \min_k \|e^{(i,j)} - e_k\|_2. \quad (1)$$

In this equation, e_k represents the embedding vectors in a shared codebook of size $\mathbb{R}^{K \times d}$, where K is the number of discrete entries or codebook vectors, and d is the dimensionality of each vector. The discrete token map q is then used to retrieve the corresponding embeddings, resulting in the embedding map e_q .

To map the tokenized representation back into the image domain, we use a decoder g_θ , which takes the embedding map e_q and generates the reconstructed output $\hat{x} := g_\theta(e_q)$. That process resembles a standard autoencoder but includes a unique non-linearity that maps latent representations to one of K embedding vectors.

During training, the codebook is initialized randomly and jointly optimized with the encoder and decoder. That adapts the codebook to the data distribution, capturing the most relevant visual features for the task.

The image tokenizer is trained using a vector quantization objective, combining reconstruction, commitment, and adversarial losses to ensure high-fidelity and perceptually realistic image reconstructions. A straight-through estimator computes the gradients, thus handling the non-differentiable nearest-neighbor lookup. For detailed formulations, see [81].

3.1.2 Auto-regressive next token predictor

The second stage of our approach generates videos in the latent space of the pre-trained Vector Quantized Variational AutoEncoder (VQ-VAE) tokenizer. We use an auto-regressive framework inspired by Large Language Model (LLM) pre-training, employing a transformer decoder to predict tokens sequentially. That allows the model to generate video content patch by patch, capturing spatial and temporal dependencies.

Objective: The model learns the conditional probability of each token given its preceding tokens. For a sequence of n tokens $\mathcal{Q} = [q^0, q^1, \dots, q^{n-1}]$, the joint distribution is factorized as the product of conditional probabilities:

$$P(\mathcal{Q}; \theta) = \prod_{i=1}^n P(q^i | q^0, q^1, \dots, q^{i-1}; \theta) \quad (2)$$

where θ are the model parameters.

We train the model to minimize the negative log-likelihood of the observed token sequences:

$$\mathcal{L}_\theta = - \sum_{i=1}^n \log P(q^i | q^0, q^1, \dots, q^{i-1}; \theta) \quad (3)$$

We use a softmax function on the model’s logits to produce a probability distribution over the vocabulary. We train the model using teacher forcing with cross-entropy loss, aligning the predicted and true token distributions.

VaViM: model architecture Building upon the previously described tokenizer discretization, we employ a GPT-2 [70] architecture to model the temporal dynamics of video tokens auto-regressively (following Equation 2). While the tokenizer’s vocabulary focuses on the perceptual compression of individual frames, our model learns a new set of embeddings optimized for capturing spatio-temporal relationships in the token sequence. Those embeddings map the tokenizer’s discrete codes q into a continuous latent space z where spatio-temporal relationships can be modeled auto-regressively.

At each layer $l \in L$, where L is the total number of layers, the computation is as follows:

$$z \leftarrow z + \text{CausalAttn}(\text{LN}(z)) \tag{4}$$

$$z \leftarrow z + \text{FFN}(\text{LN}(z)). \tag{5}$$

where $\text{FFN}(\cdot)$ denotes a fully connected layer, $\text{CausalAttn}(\cdot)$ is a causal attention layer with masking [92], and $\text{LN}(\cdot)$ denotes layer normalization [54]. We use GELU [37] as the activation function and employ weight tying between the input embedding layer and the output projection layer to reduce the number of parameters. Additionally, at inference time, a KV cache [66] is maintained for efficient auto-regressive sampling.

Following GAIA-1 [44], we use two types of learned positional embeddings to capture both spatial and temporal dependencies. The *spatial positional embedding* is shared across all frames, allowing the model to capture spatial dependencies within each image independently. In contrast, the *temporal positional embedding* is unique for each frame, enabling the model to capture dependencies across frames in a video. By combining these two positional embeddings, the model effectively learns both intra-frame and inter-frame relationships.

3.2 VaVAM = VaViM + action expert

Whether video generation pre-training effectively captures the features essential for safe and reliable driving is a key question. To bridge the gap between pre-trained video representations and driving decisions, we introduce an action expert module, forming VaVAM by complementing VaViM with decision-making. The action expert, inspired by $\pi 0$ [8], uses flow matching to generate actions by progressively denoising a noisy ego-trajectory, illustrated on the bottom left of Figure 2a, into a coherent driving trajectory. The denoising is conditioned on high-level driving commands (e.g., ‘turn left’, ‘go straight’) and video features from VaViM encoding the scene dynamics. While $\pi 0$ conditions on single frames for robotic manipulation, we extend it to driving by exploiting the temporal contexts of multiple frames that are crucial for understanding dynamic scenarios.

We adopt flow matching instead of alternatives such as action quantization [53] because it directly learns the vector fields that define the transport to the target probability distribution, enabling accurate action generation while effectively modeling complex multimodal distributions. That is particularly important for our trajectory dataset, which is challenging to capture with quantization-based methods due to its long-tail distribution dominated by straight trajectories, with maneuvers such as U-turns appearing rarely (Figure 4).

More formally, we assume a dataset of driving recordings and their associated high-level commands $\mathcal{D} = \{(O_t, A_t, c_t)\}$, with $O_t = [o_t, \dots, o_{t-N}]$ representing a sequence of images observed up to the N past frames; $c_t \in \{\text{left, right, straight}\}$ being the high-level commands, which act as a guide for the vehicle direction, e.g., ‘turn left’, on Figure 2a; and $A_t = [a_{t+1}, \dots, a_{t+H}]$ being the ‘action’, defined as a sequence of $[x, y]$ ego-positions in the BEV reference-frame specifying the dynamic profile of the driving path to undertake. We illustrate the ‘action’ trajectory at the top left of Figure 2a. The ‘action’ is extracted from the pre-recorded ego-motion over the next H future timesteps after the current timestep t .

Through the combination of VaViM and the action expert module, VaVAM effectively learns the conditional vector fields $v_\theta(A_t^\tau; O_t, c_t)$ that transport actions sampled from a noised distribution $A_t^\tau = [a_{t+1}^\tau, a_{t+2}^\tau, \dots, a_{t+H}^\tau]$ to actions A_t from the observed distribution O_t and high-level commands c_t . That denoising process is formalized in Section 4.4.

Architecture. In more detail, the action expert consists of an action encoder, a joint attention transformer, and an action decoder (Figure 2a).

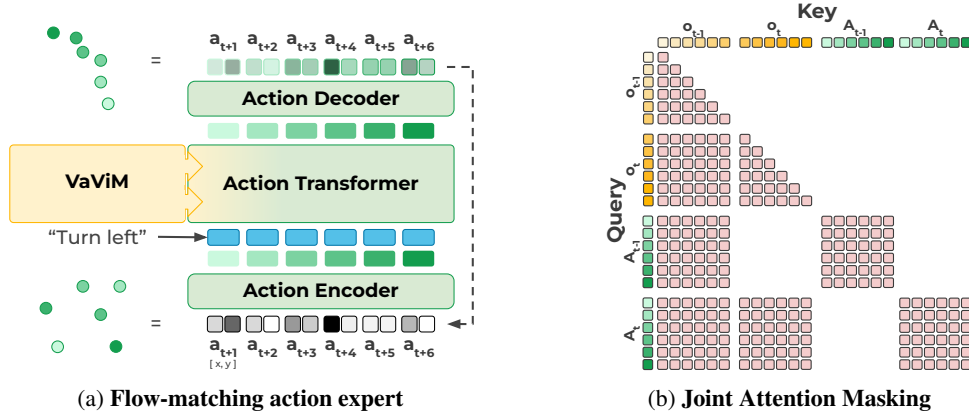


Figure 2: **Model details.** (a) The iterative denoising process for driving trajectory estimation: starting from random noise, VaViM estimates the sequence of driving waypoints (green dots), conditional to high-level commands (e.g., ‘turn left’) and VaViM features. (b) The joint attention between VaViM tokens o and action tokens A at training time.

- **Action Encoder:** It projects the actions into a latent space using an MLP and incorporates positional embeddings of the flow matching step τ , a learned temporal embedding (“action at time t ”) and a learned embedding for each high-level command (left, right, straight).
- **Joint Attention Transformer:** This module enables interaction between action representations and visual features, conditioning the denoising process on observed scene dynamics coming from VaViM. We use a specialized attention masking scheme illustrated in [Figure 2b](#)
 - Action tokens attend to all past context frames and all other action tokens within the same frame.
 - Visual tokens maintain causal masking to preserve their sequential nature, preventing them from being conditioned by future observations.
- **Action Decoder:** It maps the latent action features back to the action space with a linear layer, predicting the denoising vector field $v_\theta(A_t^T; O_t, c_t)$.

The architecture provides two key advantages. First, VaViM and the action expert interact exclusively through joint attention. This design choice allows the action expert to use a smaller MLP dimensionality than VaViM while maintaining matching dimensions in attention layers. Such dimensional reduction is crucial for efficiency, as the action expert performs multiple forward passes during iterative denoising and sampling. Second, the layer-wise joint attention addresses the challenge of feature extraction from VaViM’s layers. Different layers capture varying levels of abstraction—from raw vocabulary embeddings to task-specific features. Rather than selecting and committing to a single layer, the joint attention mechanism learns to extract relevant features across VaViM’s entire depth.

During inference, we sample trajectories by integrating the denoising vector field over 10 steps using the forward Euler method, starting from random noise $A_t^0 \sim \mathcal{N}$. That integration process progressively refines the noisy actions into a coherent driving trajectory that satisfies both the high-level command and environmental constraints captured by the temporal ∂

4 Data and Training

4.1 Data

Our desiderata for the data were to find a large dataset of non-annotated data for the pre-training and a sufficient amount of annotated data (with trajectories synchronized with perception) for fine-tuning. To that end, we train VaViM and VaVAM on a collection of three datasets: OpenDV [96], a massive non-annotated web dataset, and nuPlan [13] and nuScenes [12], dedicated automotive datasets captured with multiple sensors.

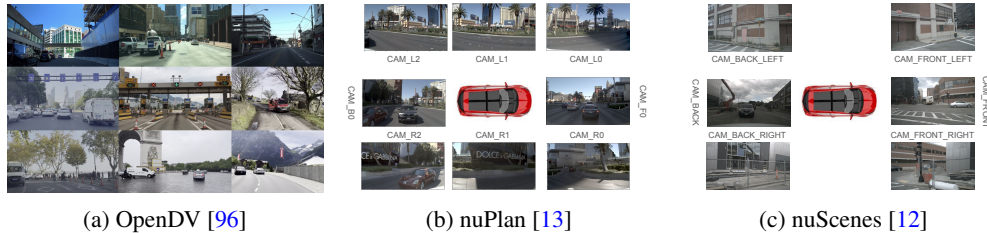


Figure 3: **Image examples.** RGB dash-cam images from (a) the OpenDV dataset [96], (b) the eight cameras in nuPlan [13], and (c) the six cameras in nuScenes [12].

OpenDV [96] The OpenDV dataset, illustrated on Figure 3a, is the largest driving dataset publicly available up to now, with more than 1700 hours of driving videos, collected at 60 FPS, resulting in over 360 million frames. The dataset comprises single-camera front-cam videos collected from YouTube, with annotated durations of intros (usually 90 seconds) and outros (usually 60 seconds) for trimming, to avoid artifacts such as title sequences and closing credits. Most videos are at or close to Full HD (1920×1080) resolution.

We include in our data only the videos at exactly Full HD to avoid issues of aspect ratio distortion. That meant discarding 1.3% of the videos (2.5% of the total duration). Using FFmpeg [82], we extracted the frames for the remaining videos at 10 FPS and 512×288 pixels, discarding intros and outros. We stored the frames in individual JPEG files. We extract overlapping clips of 8 frames at 2 FPS to train VaViM. Only a front camera is available for this dataset, without any metadata.

nuPlan [13] The nuPlan dataset contains around 1200 hours of driving scenarios recorded in Las Vegas (838 hours), Boston, Pittsburgh, and Singapore. In particular, among the 1200-hour raw data, approximately 94-hour recordings contain sensor information (LiDAR and cameras) with a sampling rate of 10 Hz. Our project only employs the RGB images in 1274 recorded videos and the ego position. More specifically, we only use the front camera instead of the eight cameras that cover the 360-degree view around the ego vehicle illustrated in Figure 3b. We collect from nuPlan 2,833,723 frames for training and 492,477 for validation, together with trajectory extracted from the ego positions. We also extract overlapping clips of 8 frames at 2 Hz from the original 10 Hz video sequences.

nuScenes [12] The nuScenes dataset contains 1000 driving scenes of 20 seconds collected in Boston and Singapore in Figure 3c. Similarly to nuPlan, while nuScenes includes 6 cameras, LiDAR, RADAR, *etc.*, we restrict its usage to the front camera and ego position in this work. That results in a dataset of 28,130 training frames and 6,019 validation frames. We also extract overlapping clips of 8 frames. The dataset is natively synchronized at 2Hz.

As detailed in subsequent sections, we use the datasets for different steps of VaViM and VaVAM training. Specifically, we use OpenDV only for VaViM pre-training Section 4.2. A mix of the three datasets to fine-tune VaViM Section 4.3. For both training steps, only the front camera is used, making those steps completely unsupervised and, thus, highly scalable. Finally, we use nuScenes and nuPlan to learn VaVAM through imitation learning on the ego trajectory Section 4.4, which are illustrated on Figure 4. That training stage requires access to the ground-truth expert trajectory, although, interestingly, recent approaches such as GEM [36], explore the use of pseudo-annotations for the ego trajectory, paving the way to scaling action learning to OpenDV-size datasets.

4.2 VaViM pre-training

Training large autoregressive models requires careful consideration of both parameterization and scaling strategy. In this section, we present our approach to efficiently scale VaViM beyond 1 billion parameters.

Compute-Efficient Scaling with μP : We adopt the Maximal Update Parametrization (μP) [95] to enable efficient scaling, inspired by recent advances in large-scale model training [45, 27, 97, 55].

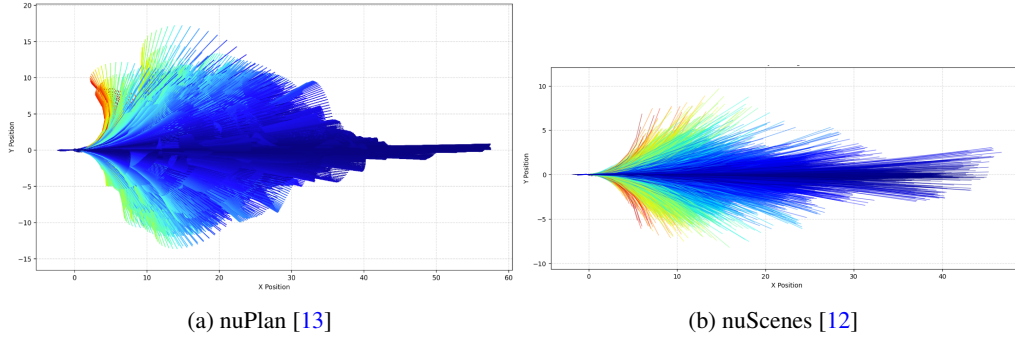


Figure 4: **Trajectory distributions.** The heading of the ego-car is oriented towards the positive y-axis. The trajectories are colored, per set of trajectories, by average yaw rate (rad/s) from blue as minimum to red as maximum. The maximum distance travelled within 3s is around 60 m in nuPlan and 40 m for nuScenes. The maximum average yaw rate is around 0.40 rad/s in nuPlan (a) and 0.25 rad/s for nuScenes (b).

μ P allows us to use the same learning rate and optimization hyperparameters across different model scales, simplifying hyperparameter tuning and stabilizing training dynamics.

μ P works by reparameterizing the network’s initialized weights, activations, and learning rate on a per-layer basis proportional to the network width. That enables width-independent updates and zero-shot hyperparameter transfer as model width scales [56, 97]¹².

We initiate hyperparameter optimization with a base model width of 256 (60M parameters). Using approximately 20% of the pre-training data, we conduct a grid search over 50 randomly sampled hyperparameter configurations, requiring around 900 GPU hours. This phase establishes the core training hyperparameters. We then scale up to a model with width 768 (185M parameters) to fine-tune the weight decay parameter, with each candidate configuration requiring about 1254 GPU hours. At this point, all hyperparameters are fixed.

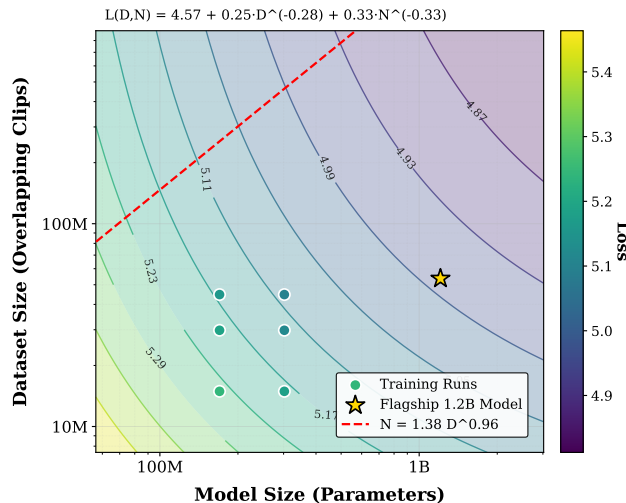


Figure 5: **VaViM scaling law** predicts the expected validation loss (next-token cross-entropy) of the 1.2B VaViM-L model and indicates that more data would strongly benefit our models. The green dots correspond to checkpoints used to fit the scaling law; the yellow star is the predicted performance of VaViM (0.06% error); the dotted red is the compute-optimal frontier [42].

¹Eleuther.ai — [muP Practitioner’s Guide](#)
²cloneofsimo — [What to do to scale up?](#)

Establishing Scaling Laws: A scaling law empirically models the validation loss as a power law of the training data and model size. Following [42], we define it as:

$$L(D, N) = L_0 + A \cdot D^{-\alpha} + B \cdot N^{-\beta}, \quad (6)$$

where:

- $L(D, N)$ is the validation loss as a function of the dataset size D and model size N .
- D is the number of video clips for training the model.
- N is the number of non-embedding model parameters.
- L_0 represents the irreducible error of an ideal model.
- $A, \alpha, B,$ and β are positive constants that capture the sensitivity to data and model size.

We estimate the parameters of the scaling law ($L_0, A, B, \alpha,$ and β) by training a model with width 1024 (318M parameters), consuming approximately 1762 GPU hours. We use the Warmup-Stable learning rate schedule [45] to extract multiple pre-trained checkpoints within one training run. Specifically, we save checkpoints at 25%, 50%, and 75% of the pre-training data for both width 768 and 1024 models.

Combining those checkpoints across different model and data scales, we fit an empirical scaling law that captures performance improvements with increasing data and model size. Using SciPy’s [91] *minimize* with the L-BFGS-B [64, 103] optimizer, we find the optimal parameters: $(L_0, A, \alpha, B, \beta) = (4.574, 0.250, 0.279, 0.326, 0.329)$. That allows us to derive the optimal scaling relationship: $D = 1.384 \cdot N^{0.962}$.

We show the scaling law isoplot and its derived optimal scaling schedule in Figure 5. Our analysis reveals that despite using the large-scale OpenDV dataset [96] with more than 1700 hours of driving data, our model is under-trained, suggesting that additional data could significantly improve performance. In total, we use 10,186 GPU hours to establish the scaling laws before the learning-rate decay phase, including 8,424 GPU hours to finalize the search of all hyperparameters. We then train the flagship model with 1.2B parameters and observe an estimation error of only 0.003 (0.06%) compared to the predicted scaling law.

4.3 Fine-tuning VaViM on target dataset

Building upon our pre-trained model, we implement a carefully designed fine-tuning strategy that leverages multiple datasets to enhance the model’s performance. Our approach begins with a checkpoint selected from the ‘stable’ phase of pre-training.

For the fine-tuning phase, we construct a diverse training mix combining three complementary datasets: (1) OpenDV, a large-scale, diverse dataset that provides broad coverage of general driving scenarios across the world; (2) nuPlan, a more specialized dataset that aligns with our subsequent imitation learning phase; (3) nuScenes, that serves the dual purpose of supporting imitation learning and targeting the NeuroNCAP evaluation, *i.e.*, the target task of driving.

From OpenDV, we initially extracted around 59M overlapping video clips and allocated 90% of them for pre-training (warmup and stable learning rate phases) and reserved the remaining 10% for fine-tuning (learning rate decay phase). However, rather than utilizing the entire fine-tuning portion, we strategically sample from multiple sources to create a balanced training mix:

- 40% from OpenDV – 2,385,300 clips
- 58.72% from nuPlan – 2,765,278 clips, representing the complete nuPlan dataset
- 1.28% from nuScenes – 76,120 clips, achieved by repeating the nuScenes dataset four times

We leave for future works to evaluate the impact of only using the 10% portion of OpenDV. An additional open question is the optimal composition of the fine-tuning data mix, possibly with different proportions of the datasets above or additional autonomous driving datasets.

4.4 Training VaVAM with imitation learning

A carefully structured imitation learning allows transforming our pre-trained video model (VaViM) into an actionable video-action model (VaVAM). This section outlines how we enable end-to-end driving capabilities while preserving the rich visual representations learned during pre-training.

As discussed in [Section 3.2](#), our approach employs flow matching, building upon the framework introduced in π_0 [8]. More formally, given a dataset of expert demonstrations with associated high-level commands $\mathcal{D} = \{(O_t, A_t, c_t)\}$, with $O_t = [o_t, \dots, o_{t-N}]$ representing the sequence of images observed up to N past frames, the high-level command $c_t \in \{\text{left, right, straight}\}$ and the expert trajectory $A_t = [a_{t+1}, \dots, a_{t+H}]$ of future positions over horizon H , we learn to denoise trajectories through a conditional probability flow.

The key insight of flow matching lies in its elegant formulation of the forward process and induced vector field. We learn a conditional denoising vector field v_θ , which defines how to progressively transform noisy trajectories back into expert-like behavior. The training process follows a forward noising schedule defined by:

$$A_t^\tau = \tau A_t + (1 - \tau)\epsilon, \quad \epsilon \sim \mathcal{N}(0, I) \quad (7)$$

That process represents a linear interpolation between the expert action A_t and Gaussian noise ϵ . The variable $\tau \in [0, 1]$ represents the noise level. This process smoothly interpolates between expert actions ($\tau = 0$) and pure noise ($\tau = 1$) and traces out paths in the action manifold. For training, the action expert uses the following objective to predict the denoising vector field v_θ :

$$L^\tau(\theta) = \mathbb{E}_{p(A_t|O_t, c_t), q(A_t^\tau|A_t)} \|v_\theta(A_t^\tau, O_t, c_t) - u(A_t^\tau|A_t)\|^2 \quad (8)$$

where $q(A_t^\tau|A_t)$ is the forward process defined above and $u(A_t^\tau|A_t)$ is the optimal transport vector field. The optimal transport vector field $u(A_t^\tau|A_t)$ represents the ideal direction in which noisy actions should move to become expert actions. Our learned vector field v_θ approximates this optimal transport. The vector field acts as the generator of a continuous transformation on the manifold of plausible driving actions. It generates a flow that transforms a simple distribution (Gaussian noise) into our target distribution of expert actions. During inference, we generate action sequences by integrating the learned vector field:

$$A_t^{\tau+\delta} = A_t^\tau + \delta \cdot v_\theta(A_t^\tau, O_t, c_t) \quad (9)$$

using 10 steps of the forward Euler method, starting from random noise $A_t^0 \sim \mathcal{N}(0, I)$.

That framework enables our model to capture complex multimodal action distributions directly from the expert demonstration. The effectiveness of this approach is extensively demonstrated in [Section 5.2](#), where we show strong performance in both open-loop prediction and closed-loop driving scenarios.

4.5 Implementation and Training details

Tokenizer. We use a pre-trained image tokenizer, LlamaGen [81], which is based on the VQGAN architecture. Specifically, we use the stride=16 tokenizer, which has 72M parameters. It has a vocabulary size of 16,384 with codewords of 8 dimensions. We use images of size 512×288 , resulting in a token map of 32×18 , or 576 tokens.

VaViM is based off a GPT-2 transformer architecture [70]. We train it with a context length of 8 frames, resulting in a maximum context of 4,608 tokens. It has 24 layers, a vocabulary size of 16,384, with a width scaling from 768 (VaViM-S) to 1024 (VaViM-B), up to 2048 (VaViM-L). This results in a codebook of size 12.6M, 16.8M, and 33.65M respectively. We keep the dimensionality of the heads fixed at 128, making the number of attention heads scale with the model size. We set a standard multiplication factor of 4 for the FFN hidden dimensionality. We optimize it with AdamW [60], a base learning rate of 0.0041, a weight decay of $1e-7$, and $\beta = (0.9, 0.95)$ while clipping the gradient with a norm of 1.0. Finally, we initialize with a standard deviation of 0.0289. As described in [Section 4.2](#), the μP parameterization scales the learning rate per layer according to the width layer (see our code or [95] from exact specifications). We train all our models with a batch size of 384 and vary the number of GPUs depending on the model size to maximize GPU utilization.

Table 2: Evaluation of video generation quality on KITTI [32] and nuScenes [12]. FID@t is the generation FID on the t -th frame (lower is better). Larger models tend to have better FIDs. The FIDs are within the ballpark of the upper bound given by the ‘oracle’ implemented with LlamaGen [81].

MODEL	# PARAMS	KITTI [32]				NUSCENES [12]			
		FID@1	FID@2	FID@3	FID@4	FID@1	FID@2	FID@3	FID@4
Oracle upper-bound									
LLAMAGEN	-	6.8	7.4	7.7	8.1	9.8	9.9	10.2	10.4
Fine-tuned									
VAVIM-S	185M	15.1	22.1	28.3	34.5	23.9	30.8	35.8	39.8
VAVIM-B	318M	13.7	19.5	24.6	30.0	20.7	27.5	33.2	38.6
VAVIM-L	1.2B	12.0	16.4	20.8	24.7	16.8	19.6	23.2	26.1

VaVAM predicts the trajectory for the 6 next timesteps at 2 Hz, *i.e.*, for 3 seconds. The dimensionality of VaVAM attention layers is identical to its VaViM companion for the joint attention (Section 3.2). However, VaVAM’s MLP layers dimensionality is reduced by a factor of 4 with respect to VaViM’s dimensionality for efficient action sampling; *i.e.* 192 for VaVAM-S, 256 for VaVAM-B, and 512 for VaViM-L. For the joint attention, we must project the tokens to match the VaViM’s dimensionality. We use a learning rate equal to 0.0194, an initialization standard deviation of 0.0086, and similar optimizer parameters to VaViM. For the flow matching loss, we follow π_0 and use a beta distribution for the noise schedule and 10 steps for denoising at inference time. We efficiently train our model with different observation context lengths using a block attention pattern (Figure 2b). That allows training the action expert to handle varying lengths of temporal context from one training clip.

Training infrastructure. We detail the compute requirements for our most compute-intensive run, training VaViM-L. We run our training on 48 nodes of 4 H100s, totaling 192 GPUs. To help scale that job, we employ lightning [30] and deepspeed-stage2 [73]. The total running time for the training is around 25 hours, totaling around 4800 (H100) GPU hours. We pre-train the model on approximately 60 million overlapping windows.

5 Experiments and Results

Additional evaluation datasets. We evaluate VaViM and VaVAM on datasets not used for their training, namely Cityscapes [23] and KITTI [32]. We refer to the latter as *KITTI* when we downsample the clips to 8 frames at 2 Hz (to match the training FPS) and as *KITTI-1f* when we downsample the clips to a single frame.

5.1 VaViM video pre-training evaluation

5.1.1 Generation quality

To evaluate the quality of the generation of our VaViM, we use the Frechet Inception Distance (FID) [38]. To account for non-object-centric settings typical of driving datasets, we use the features from a DINOv2 model, which have been shown to be richer.

Specifically, given a context of 4 frames, we generate 4 frames with VaViM. We use the features of the 4 context frames as reference images to compute the FID. We compute an FID score for each future frame individually (FID@t), *i.e.*, FID@2 means the FID of the second generated frame. Since VaViM does not directly generate images but tokens, we compute the FID for the LLamaGen-VQGAN tokenizer to act as an upper bound, as it serves as an ‘oracle’, *i.e.*, it encodes a real frame of the ‘future’. We choose the same reference frames for the FID. And compute the FID individually for the 4 ground-truth future frames. That setting changes slightly compared to the reconstruction FID, as the features of the original images considered for reconstruction are not part of the reference images used to compute the FID. Note that, although we pre-train on a video clip, we do not use Frechet Video Distance [86] (FVD) for evaluation because it relies on an I3D [15] that requires at least 10 frames as input.

Table 3: Evaluating VaViM on zero-shot semantic segmentation with Humming-Bird [5] on Cityscapes [23] and KITTI [32]. Results in mIoU (higher is better).

MODEL	# PARAMS (in M)	CITYSCAPES [23]	KITTI-1F [32]	KITTI [32]
Baseline Models				
DINOv1-B [14]	85	31.5	34.7	35.1
DINOv2-B [65]	86	43.4	41.8	41.6
DINOv2-L [65]	300	13.0	16.5	16.7
DINOv2-G [65]	1100	37.8	40.9	40.6
Pre-trained				
VAViM-S	185	20.0	25.5	22.1
VAViM-B	318	21.2	25.1	23.3
VAViM-L	1200	17.9	21.0	20.4
Fine-tuned				
VAViM-S	185	20.3	25.4	23.2
VAViM-B	318	20.8	25.3	23.4
VAViM-L	1200	18.4	22.0	20.3

From Table 2, we observe a clear scaling benefit, where larger models consistently achieve better performance, where VaViM-L outperforms VaViM-B, which further outperforms VaViM-S. That trend highlights the advantage of increasing model capacity to improve reconstruction quality and other evaluation metrics.

We also show qualitative results for generation on Figure 6. We feed a context of 4 frames Figure 6a to either VaViM-S Figure 6b or VaViM-L Figure 6c. We observe that both models generate frames that are spatially coherent, with correctly generated large structures. Furthermore, we observe that VaViM-L predicts frames closer to the true future (car on the left turning right) by inferring the motion from the 4 first frames. That contrasts with the generative behavior of VaViM-S.

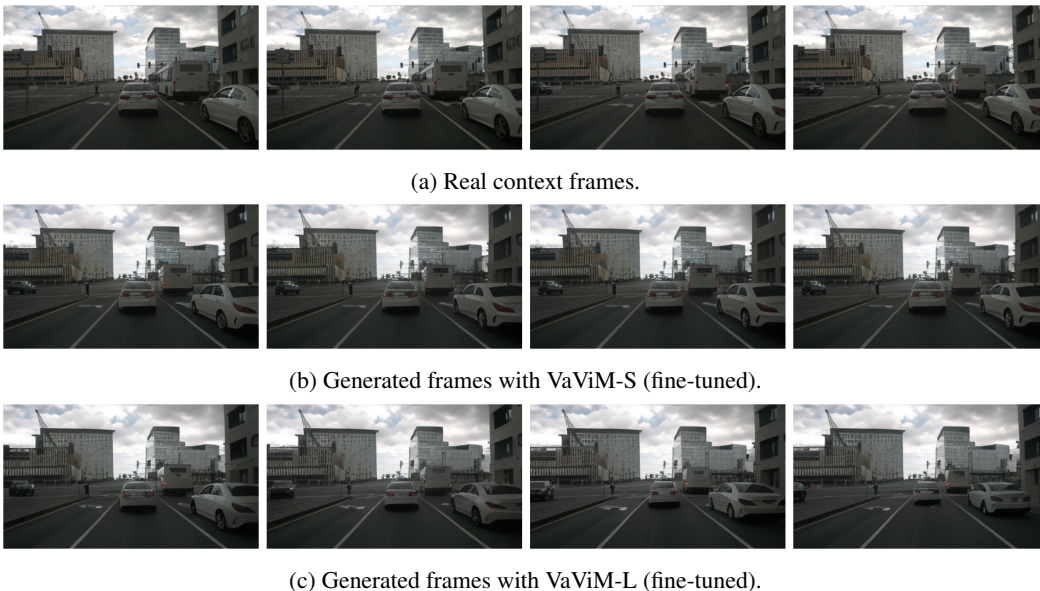


Figure 6: **Video generation with VaViM.** Given 4 context frames (a), we generate the next 4 frames with VaViM-S (b) and VaViM-L (c). Both models correctly predict the overall structure, but only VaViM-L generates the expected motion.

5.1.2 Semantic segmentation

In [Table 3](#), we evaluate VaViM for semantic segmentation using the Humming-bird approach [\[5\]](#). Specifically, we use the features of layer 12 of our VaViM’s transformer to encode a frame. We sample 10 patch-features per image, using the sampling approach of the open-source Humming-bird implementation [\[67\]](#). We report the mean Intersection over Union (mIoU), which measures the overlap between predicted and ground truth segmentations across all classes, providing a comprehensive assessment of per-class and overall segmentation quality. Higher mIoU scores indicate better alignment with ground-truth annotations.

As observed in recent studies [\[71\]](#), auto-regressive models struggle compared to discriminative models like Dino and Dinov2 [\[14, 65\]](#). We can see Dino models outperform VaViM on all setups. However, this study shows that, even with the auto-regressive pre-training that does not explicitly enforce semantic understanding, VaViM still manages to segment the different datasets in a zero-shot manner: indeed, neither Cityscapes nor KITTI was part of the training data mix. [Table 3](#) also shows that during fine-tuning on our target datasets, VaViM does not lose the representation capability learned on the diverse pre-training data.

Moreover, we conduct a qualitative study on the features obtained with VaViM on [Figure 7](#). As proposed by [\[14\]](#), we visualize as RGB primaries the 3 main components of a PCA of the features. The semantic consistency of VaViM’s is visible as similar colors being assigned to objects of the same class (*e.g.*, pedestrians, cars, or road), which suggests the features hold semantic meaning, even if they are not invariant enough to perform at semantic segmentation.



Figure 7: **Main components of VaViM’s representation.** We take features from VaViM’s 22nd layer, project them with PCA, and map the three main components to the RGB primaries. The features have a considerable semantic grouping, shown as objects of the same type (pedestrians, cross-walk, road markings, cars, etc.) being assigned similar colors.

5.2 VaVAM driving evaluation

5.2.1 Open-loop evaluation

In [Table 4](#), we evaluate VaVAM in an open-loop setup. We compute the $\min\text{ADE}_k$ (\downarrow), *i.e.*, the minimum over k sampled trajectories of the Average Distance Error, taken as the average of point-wise L^2 distances between the closest (among $k = 5$) sampled trajectory and the ground-truth expert trajectory. The metric is calculated for both nuPlan [\[13\]](#) and nuScenes [\[12\]](#).

Table 4: Open-loop evaluation of VaVAM measured with minADE_k (\downarrow), with $k = 5$. Increasing compute (bigger models, more data) results in a lower minADE. The parameter counts of our models appear as <parameters in VaViM> + <parameters in the action expert of VaVAM>.

MODEL	# PARAMS (IN M)	# DATA (in $\times 10^3$)	NUSCENES [12]	NUPLAN [13]
Video-action models trained from raw data				
		38	1.14	0.76
VAVAM-S	185 + 21	77	1.13	0.83
		116	1.04	0.77
		139	1.00	0.68
VAVAM-B	318 + 38	38	0.96	0.57
		77	0.93	0.59
		116	0.95	0.64
		139	0.85	0.53
VAVAM-L	1,200 + 150	139	0.80	0.52

We observe a clear trend where scaling improves minADE, which shows that among the different samples, VaVAM is able to match the expert ones better when increasing the compute ($\sim \# \text{ params} \times \# \text{ data}$). Qualitatively, we observe that as smoother trajectories for “better” models. However, as evidenced by prior works [22, 24] and our results in closed-loop evaluation (Section 5.2.2), open-loop scores are not predictive of good driving capabilities.

5.2.2 Closed-loop evaluation

NeuroNCAP: While the previous open-loop evaluation demonstrates strong trajectory prediction accuracy, it fails to capture the cascading effects of the model’s decisions. Closed-loop evaluation addresses that limitation by allowing decisions to influence future observations, thus providing a more realistic assessment of safety-critical behavior.

To evaluate our model’s performance in closed-loop, we employ NeuroNCAP [59], a simulator specifically designed for testing autonomous driving systems in safety-critical scenarios. To the best of our knowledge, it is currently the only existing data-based closed-loop simulator. Other solutions are either synthetic [28] (leading to domain gap) or based on view reprojection [2, 3] (leading to limited novel views).

NeuroNCAP employs a NeRF-based simulator that executes the driving model decision and generates the corresponding novel view. That enables photorealistic closed-loop evaluation of driving models. In particular, a key feature of NeuroNCAP is its ability to insert pre-defined adversarial agents into the scene, such as a vehicle following hazardous trajectories.

Using that capability, the framework creates challenging test conditions inspired by the European New Car Assessment Programme (Euro NCAP), featuring three primary scenario types: stationary obstacles in the ego-lane, frontal collisions with oncoming vehicles, and side collision scenarios from cross-traffic. In our experiments, we leverage this framework to systematically evaluate our VaVAM model’s ability to handle those challenging scenarios while maintaining its intended trajectory.

Collision metrics: NeuroNCAP’s evaluation protocol relies on two metrics: (1) the collision rate as a percentage of scenarios without collision and (2) the NeuroNCAP score (NNS) that assigns scores based on collision avoidance success and impact velocity reduction, offering a quantitative measure of the model’s safety performance. More formally:

$$\text{NNS} = \begin{cases} 5.0 & \text{if no collision} \\ 4.0 \cdot \max(0, 1 - v_i/v_r) & \text{otherwise} \end{cases} \quad (10)$$

Baselines: We first compare VaVAM with existing NeuroNCAP baselines. The Base-U and Base-V baselines are naïve methods that use the perception outputs from UniAD [47] and VAD [48], respectively. They operate on a simple rule-based approach: maintaining constant velocity unless

Table 5: Performance on Neuro-NCAP benchmark. VaVAM obtains SOTA scores on the frontal scenarios, despite using only a front-cam and no human annotations. We highlight the post-processing step and the side scenario in gray to emphasize that VaVAM does not use post-processing of the trajectories [47] and only uses the frontal camera as input, while other methods have 360° perception. Scores with † were reproduced by us.

MODEL	POST-PROC.	NEURONCAP SCORE ↑				COLLISION RATE (%) ↓			
		AVG.	STAT.	FRONTAL	SIDE	AVG.	STAT.	FRONTAL	SIDE
Baseline Model trained w/ hand-labeled annotations									
BASE-U	-	2.65	4.72	1.80	1.43	69.90	9.60	100.00	100.00
BASE-V	-	2.67	4.82	1.85	1.32	68.70	6.00	100.00	100.00
UNIAD	✗	0.73	0.84	0.10	1.26	88.60	87.80	98.40	79.60
VAD	✗	0.66	0.47	0.04	1.45	92.50	96.20	99.60	81.60
UNIAD	✓	1.84	3.54	0.66	1.33	68.70	34.80	92.40	78.80
UNIAD†	✓	2.08	3.58	1.18	1.48	61.1	31.2	78.8	73.2
VAD	✓	2.75	3.77	1.44	3.05	50.70	28.70	73.60	49.80
Video-action model trained from raw data									
VAVAM-L	✗	2.46	3.55	2.38	1.47	57.90	41.40	56.80	75.60

an object is detected in a corridor ahead of the ego-vehicle (± 2 meters laterally and up to $2*v_{ego}$ meters longitudinally). If an object is detected within this corridor ($TTC < 2s$), they initiate a braking maneuver. The second class of baselines are state-of-the-art end-to-end planners, UniAD [47] and VAD [48], which process 360° camera input, CAN-bus signals, and high-level commands to predict future trajectories.

A quantitative comparison appears in Table 5. Traditional baseline models establish a strong foundation in static scenarios, with Base-U and Base-V achieving NeuroNCAP scores of 4.72 and 4.82, respectively, setting a robust performance threshold for advanced approaches to surpass.

VAD demonstrates superior overall performance, achieving a 12% reduction in collision rates compared to our approach across all test conditions. Our qualitative assessment reveals that while VaVAM effectively identifies and responds to dynamic obstacles, it seldom initiates complete stops or urgent braking, even in scenarios where such actions would be optimal, such as encountering a stationary bus in the middle of the road.

Neither VaViM nor VaVAM predicts occupancy, which was shown to boost performances when used to post-process estimated trajectories [59], by allowing optimization with a classical solver. Such post-processing might also benefit VaVAM. Moreover, VaVAM currently relies exclusively on front-cam input, giving it an inherent disadvantage against systems with 360 camera arrays, especially for side-impact scenarios. Despite those limitations, VaVAM demonstrates competitive capabilities, notably surpassing UniAD’s in side scenarios by 4%. In frontal scenarios, VaVAM achieves state-of-the-art performance, with a NeuroNCAP score of 2.38.

Limitations of the benchmark: We unintentionally produced a noisy model that avoided the road, as it never encountered the scripted hazardous scenarios, it achieved exceptionally high safety scores in the benchmark (> 4.0 NNS). That finding highlights a critical gap in the evaluation framework: while it effectively measures collision avoidance, it does not adequately assess adherence to intended driving behavior or route completion metrics.

To address those limitations and provide a more comprehensive evaluation, we propose to use two complementary metrics. First, we measure the mean deviation from the guiding trajectory, which quantifies how well the model adheres to intended driving paths. It differs from the ADE metrics by measuring the mean instantaneous distance to the closest point of the reference trajectory instead of ADE’s pairwise distance. Second, we introduce a goal-progress metric that measures the relative reduction in distance to the destination, formally defined as:

$$\text{progress_toward_goal} = \max(0.0, \frac{d_{\text{initial}} - d_{\text{final}}}{d_{\text{initial}}}) \quad (11)$$

where d_{initial} and d_{final} represent the initial and final distances to the goal, respectively. That formulation ensures the metric remains bounded between 0 and 1, where 1 indicates complete goal

Table 6: Extended NeuroNCAP scores for the frontal scenario using mean deviation and progress (Equation 11) as additional metrics. We reproduce the scores of UniAD [47]. The parameter counts of our models appear as <parameters in VaViM> + <parameters in the action expert of VaVAM >.

MODEL	# PARAMS (IN M)	# DATA (in K)	NNS \uparrow	COLL. RATE (%) \downarrow	MEAN DEVIATION \downarrow	PROGRESS (%) \uparrow
Baseline Model trained w/ hand-labeled annotations						
UniAD [47]	-	-	1.18	78.8	1.077	47.1
Video-action models trained from raw data						
VAVAM-S	185 + 21	38	3.019	44.4	2.616	39.8
		77	3.022	44.8	2.486	40.8
		116	2.795	48.4	2.394	42.4
		139	2.669	50.0	2.022	42.5
VAVAM-B	318 + 38	38	2.585	53.6	1.686	40.9
		77	2.218	62.4	1.489	38.7
		116	2.814	48.4	2.004	39.6
VAVAM-L	1,200 + 150	139	1.781	70.0	1.234	39.7
			2.375	56.80	1.541	40.2

achievement. Together, those metrics effectively capture both the quality of trajectory following and task completion, providing a more robust framework for evaluating autonomous driving systems that prevent the gaming of safety metrics through undesirable driving behaviors.

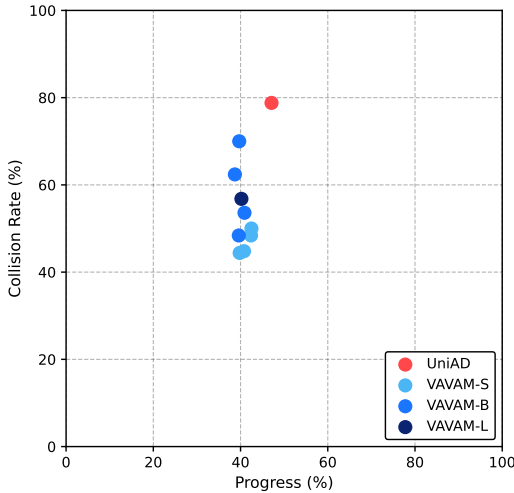


Figure 8: **Collision Rate vs. Progress.** An ideal model would be positioned at the bottom right corner of this plot, attaining the defined goal position without any collisions. VaVAM makes progress towards that ideal by being safer than UniAD, with 27% less collisions, with minimal degradation to progress.

facing an adversarial vehicle, the model must simultaneously respect that learned behavior (following the trajectory) while adapting to a situation that may require significant deviation from it (avoiding collision).

Using those metrics, we study the behavior of VaVAM in Table 6. We focus on the score of the frontal scenario as our model is front-cam only. We plot the collision rate vs progress in Figure 8. Although our model significantly reduces collision rate, it only achieves comparable collision rate to UniAD. We expected that as we scale the model and training data, our model would be able to increase the progress score while improving metrics related to collisions (NeuroNCAP score and collision rate). However, as we scale, whether in data or model size, the progress metric varies unpredictably, and the collision rate tends to increase. At the same time, we observe that the mean deviation decreases.

We hypothesize that such a phenomenon is mainly due to the limitations of the imitation learning methodology and the definition of the high-level command. Indeed, the model is trained exclusively through imitation learning on pre-recorded expert trajectories, which serve a dual purpose: as training data and as a guiding signal during training and inference.

During training, the model learns to follow exactly the trajectories presumably executed safely by expert drivers. However, at test time, when

As the training compute scales up, collision rate increases and the mean deviation metric decreases, which suggests that larger and more trained models may be overfitting to the trajectory-following behavior. Rather than learning the underlying decision-making process that still allows for safe deviation, the model becomes more rigid in its adherence to the guiding trajectory.

6 Conclusion

VaViM and VaVAM are a significant step forward in applying large-scale unlabeled pre-training to autonomous driving, offering several exciting discoveries. First, the successful transfer of the pre-trained representations to driving tasks demonstrates the versatility of our approach. Complex driving behaviors are learned directly from raw video without requiring expensive semantic annotations. Particularly encouraging is VaVAM’s reduction of existing methods’ collision rates by 27% while maintaining comparable progress metrics. Second, the performance on out-of-distribution datasets like KITTI and Cityscapes demonstrates our approach’s robustness and generalization capabilities. Third, our scaling experiments reveal a clear path forward. The empirical scaling laws we established suggest substantial headroom for improvement, notably through increased training data.

By releasing our complete codebase, training recipes, scaling laws, and model weights, we aim to accelerate progress in video-based autonomous driving. We envision several promising directions for future work:

- Decoupling high-level command path from actual expert trajectory so that, in the imitation training set, the model observes the expert deviating from the high-level command path.
- Extending our approach to leverage multi-camera setups for enhanced scene understanding.
- Exploring more sophisticated action generation frameworks that maintain the benefits of our current approach while improving safety-critical behavior.
- Investigating larger-scale pre-training on even more diverse driving datasets.
- Using a better tokenizer than the current LLaMaGen-VQGAN, adapted to driving scenarios and better able to capture fine visual details (text on signs, road markings, traffic lights, etc.).

The key limitation of our work lies in the gap between VaViM’s ability to model future states and VaVAM’s current reliance on imitation learning. While VaViM can generate plausible future video streams, we have not yet leveraged that predictive power for planning and control. A critical missing piece is a reward model that distinguishes between favorable and critical latent states, enabling more sophisticated planning strategies beyond pure imitation. That presents an exciting opportunity to transform our reactive system into a proper ‘world-model’-based planning pipeline.

Additionally, while comprehensive for driving performance, our evaluation framework does not fully evaluate the depth of physical understanding learned by our video model. Future work should develop more nuanced evaluation metrics, similar to Physics-IQ [63]’s spatial and temporal mIoU approach to assess different aspects of physical understanding. Such metrics would provide deeper insights into what our models learn about scene dynamics, object interactions, and physical constraints.

Acknowledgements

This work was partially supported by the ANR MultiTrans project (ANR-21-CE23-0032). It was initially explored using HPC resources from GENCI–CINES (Grant 2023-A0141014181), and most of its results were obtained using HPC resources from GENCI–IDRIS (Grant 2024-GC011015459). We acknowledge the EuroHPC Joint Undertaking for awarding this project access to the EuroHPC supercomputer LEONARDO, hosted by CINECA (Italy) and the LEONARDO consortium, through a EuroHPC AI and Data-Intensive Access call.

Detailed Contributions

PROJECT LEAD

Research direction, technical roadmap, and project coordination

Florent Bartoccioni

CORE CONTRIBUTORS

All aspects of the codebase, experiments, and evaluations

Florent Bartoccioni, Elias Ramzi

CONTRIBUTORS

Victor Besnier — *Visual Tokenization codebase using pre-trained VQGAN; FID metric code*

Loick Chambon — *Data download, transfer and extraction; visualization code development*

Eduardo Valle — *OpenDV preprocessing*

Shashanka Venkataramanan — *Depth anything pseudo-GT generation*

Tuan-Hung Vu — *GPT adaptation from nanoGPT*

Yihong Xu — *nuPlan preprocessing and initial dataloader development*

TECHNICAL REPORT

Manuscript preparation, design, visualizations, figures

Florent Bartoccioni, Elias Ramzi, Victor Besnier, Shashanka Venkataramanan, Eloi Zablocki, Yihong Xu, Tuan-Hung Vu, Eduardo Valle

GRANT ACQUISITIONS

Grant proposals for Adastra, EuroHPC, and Jean Zay Grand Challenges

Florent Bartoccioni, Alexandre Boulch, Mickael Chen, Eduardo Valle, Spyros Gidaris, Eloi Zablocki, Matthieu Cord, Serkan Odabas, David Hurych

ADVISORY

Research and organization guidance

Eloi Zablocki, Alexandre Boulch, Mickael Chen

SENIOR ADVISORY

Research and organization guidance

Eduardo Valle, Andrei Bursuc, Renaud Marlet, Matthieu Cord

References

- [1] Eloi Alonso, Adam Jelley, Vincent Micheli, Anssi Kanervisto, Amos Storkey, Tim Pearce, and François Fleuret. Diffusion for world modeling: Visual details matter in atari. In *NeurIPS*, 2024.
- [2] Alexander Amini, Igor Gilitschenski, Jacob Phillips, Julia Moseyko, Rohan Banerjee, Sertac Karaman, and Daniela Rus. Learning robust control policies for end-to-end autonomous driving from data-driven simulation. *IEEE Robotics and Automation Letters*, 2020.
- [3] Alexander Amini, Tsun-Hsuan Wang, Igor Gilitschenski, Wilko Schwarting, Zhijian Liu, Song Han, Sertac Karaman, and Daniela Rus. Vista 2.0: An open, data-driven simulator for multimodal sensing and policy learning for autonomous vehicles. In *ICRA*, 2022.
- [4] Bowen Baker, Ilge Akkaya, Peter Zhokhov, Joost Huizinga, Jie Tang, Adrien Ecoffet, Brandon Houghton, Raul Sampedro, and Jeff Clune. Video pretraining (VPT): learning to act by watching unlabeled online videos. In *NeurIPS*, 2022.
- [5] Ivana Balazevic, David Steiner, Nikhil Parthasarathy, Relja Arandjelovic, and Olivier J. Hénaff. Towards in-context scene understanding. In *NeurIPS*, 2023.
- [6] Chris Bamford and Simon M. Lucas. Neural game engine: Accurate learning of generalizable forward models from pixels. In *IEEE CoG*, 2020.
- [7] Lucas Beyer, Andreas Steiner, André Susano Pinto, Alexander Kolesnikov, Xiao Wang, Daniel Salz, Maxim Neumann, Ibrahim Alabdulmohsin, Michael Tschannen, Emanuele Bugliarello, Thomas Unterthiner, Daniel Keysers, Skanda Koppula, Fangyu Liu, Adam Grycner, Alexey A. Gritsenko, Neil Houlsby, Manoj Kumar, Keran Rong, Julian Eisenschlos, Rishabh Kabra, Matthias Bauer, Matko Bosnjak, Xi Chen, Matthias Minderer, Paul Voigtlaender, Ioana Bica, Ivana Balazevic, Joan Puigcerver, Pinelopi Papalampidi, Olivier J. Hénaff, Xi Xiong, Radu Soricut, Jeremiah Harmsen, and Xiaohua Zhai. Paligemma: A versatile 3b VLM for transfer. *CoRR*, 2024.

- [8] Kevin Black, Noah Brown, Danny Driess, Adnan Esmail, Michael Equi, Chelsea Finn, Niccolo Fusai, Lachy Groom, Karol Hausman, Brian Ichter, Szymon Jakubczak, Tim Jones, Liyiming Ke, Sergey Levine, Adrian Li-Bell, Mohith Mothukuri, Suraj Nair, Karl Pertsch, Lucy Xiaoyang Shi, James Tanner, Quan Vuong, Anna Walling, Haohuan Wang, and Ury Zhilinsky. π^0 : A vision-language-action flow model for general robot control, 2024.
- [9] Andreas Blattmann, Robin Rombach, Huan Ling, Tim Dockhorn, Seung Wook Kim, Sanja Fidler, and Karsten Kreis. Align your latents: High-resolution video synthesis with latent diffusion models. In *CVPR*, 2023.
- [10] Tim Brooks, Bill Peebles, et al. Video generation models as world simulators. *OpenAI*, 2024.
- [11] Jake Bruce, Michael Dennis, Ashley Edwards, Jack Parker-Holder, Yuge Shi, Edward Hughes, Matthew Lai, Aditi Mavalankar, Richie Steigerwald, Chris Apps, Yusuf Aytar, Sarah Bechtle, Feryal Behbahani, Stephanie Chan, Nicolas Heess, Lucy Gonzalez, Simon Osindero, Sherjil Ozair, Scott Reed, Jingwei Zhang, Konrad Zolna, Jeff Clune, Nando de Freitas, Satinder Singh, and Tim Rocktäschel. Genie: Generative interactive environments, 2024.
- [12] Holger Caesar, Varun Bankiti, Alex H. Lang, Sourabh Vora, Venice Erin Liong, Qiang Xu, Anush Krishnan, Yu Pan, Giancarlo Baldan, and Oscar Beijbom. nuscenec: A multimodal dataset for autonomous driving. In *CVPR*, 2020.
- [13] Holger Caesar, Juraj Kabzan, Kok Seang Tan, Whye Kit Fong, Eric M. Wolff, Alex H. Lang, Luke Fletcher, Oscar Beijbom, and Sammy Omari. nuplan: A closed-loop ml-based planning benchmark for autonomous vehicles. *CoRR*, 2021.
- [14] Mathilde Caron, Hugo Touvron, Ishan Misra, Hervé Jégou, Julien Mairal, Piotr Bojanowski, and Armand Joulin. Emerging properties in self-supervised vision transformers. *ICCV*, 2021.
- [15] João Carreira and Andrew Zisserman. Quo vadis, action recognition? A new model and the kinetics dataset. In *CVPR*, 2017.
- [16] Huiwen Chang, Han Zhang, Lu Jiang, Ce Liu, and William T. Freeman. Maskgit: Masked generative image transformer. In *CVPR*, 2022.
- [17] Hila Chefer, Uriel Singer, Amit Zohar, Yuval Kirstain, Adam Polyak, Yaniv Taigman, Lior Wolf, and Shelly Sheynin. Videojam: Joint appearance-motion representations for enhanced motion generation in video models. *CoRR*, 2025.
- [18] Li Chen, Penghao Wu, Kashyap Chitta, Bernhard Jaeger, Andreas Geiger, and Hongyang Li. End-to-end autonomous driving: Challenges and frontiers. *IEEE TPAMI*, 2024.
- [19] Long Chen, Oleg Sinavski, Jan Hünermann, Alice Karnsund, Andrew James Willmott, Danny Birch, Daniel Maund, and Jamie Shotton. Driving with llms: Fusing object-level vector modality for explainable autonomous driving. In *ICRA*, 2024.
- [20] Mark Chen, Alec Radford, Rewon Child, Jeffrey Wu, Heewoo Jun, David Luan, and Ilya Sutskever. Generative pretraining from pixels. In *ICML*, 2020.
- [21] Kashyap Chitta, Aditya Prakash, Bernhard Jaeger, Zehao Yu, Katrin Renz, and Andreas Geiger. Transfuser: Imitation with transformer-based sensor fusion for autonomous driving. *PAMI*, 2023.
- [22] Felipe Codevilla, Antonio M López, Vladlen Koltun, and Alexey Dosovitskiy. On offline evaluation of vision-based driving models. In *ECCV*, 2018.
- [23] Marius Cordts, Mohamed Omran, Sebastian Ramos, Timo Rehfeld, Markus Enzweiler, Rodrigo Benenson, Uwe Franke, Stefan Roth, and Bernt Schiele. The cityscapes dataset for semantic urban scene understanding. In *CVPR*, 2016.
- [24] Daniel Dauner, Marcel Hallgarten, Andreas Geiger, and Kashyap Chitta. Parting with misconceptions about learning-based vehicle motion planning. In *CoRL*, 2023.
- [25] Daniel Dauner, Marcel Hallgarten, Tianyu Li, Xinshuo Weng, Zhiyu Huang, Zetong Yang, Hongyang Li, Igor Gilitschenski, Boris Ivanovic, Marco Pavone, Andreas Geiger, and Kashyap Chitta. Navsim: Data-driven non-reactive autonomous vehicle simulation and benchmarking. In *NeurIPS*, 2024.
- [26] Jacob Devlin, Ming-Wei Chang, Kenton Lee, and Kristina Toutanova. BERT: pre-training of deep bidirectional transformers for language understanding. In Jill Burstein, Christy Doran, and Thamar Solorio, editors, *NAACL-HLT*, 2019.

- [27] Nolan Dey, Gurpreet Gosal, Zhiming Chen, Hemant Khachane, William Marshall, Ribhu Pathria, Marvin Tom, and Joel Hestness. Cerebras-gpt: Open compute-optimal language models trained on the cerebras wafer-scale cluster. *CoRR*, 2023.
- [28] Alexey Dosovitskiy, Germán Ros, Felipe Codevilla, Antonio M. López, and Vladlen Koltun. CARLA: an open urban driving simulator. In *CoRL*, 2017.
- [29] Patrick Esser, Robin Rombach, and Björn Ommer. Taming transformers for high-resolution image synthesis. In *CVPR*, 2020.
- [30] William Falcon and The PyTorch Lightning team. PyTorch Lightning, March 2019.
- [31] Shenyuan Gao, Jiazhi Yang, Li Chen, Kashyap Chitta, Yihang Qiu, Andreas Geiger, Jun Zhang, and Hongyang Li. Vista: A generalizable driving world model with high fidelity and versatile controllability. In *NeurIPS*, 2024.
- [32] Andreas Geiger, Philip Lenz, Christoph Stiller, and Raquel Urtasun. Vision meets robotics: The KITTI dataset. *IJRR*, 2013.
- [33] Ian Goodfellow, Jean Pouget-Abadie, Mehdi Mirza, Bing Xu, David Warde-Farley, Sherjil Ozair, Aaron Courville, and Yoshua Bengio. Generative adversarial networks. *ACM*, 2020.
- [34] Cole Gulino, Justin Fu, Wenjie Luo, George Tucker, Eli Bronstein, Yiren Lu, Jean Harb, Xinlei Pan, Yan Wang, Xiangyu Chen, John D. Co-Reyes, Rishabh Agarwal, Rebecca Roelofs, Yao Lu, Nico Montali, Paul Mougín, Zoey Yang, Brandyn White, Aleksandra Faust, Rowan McAllister, Dragomir Anguelov, and Benjamin Sapp. Waymax: An accelerated, data-driven simulator for large-scale autonomous driving research. In *NeurIPS - Track on Datasets and Benchmarks*, 2023.
- [35] Xi Guo, Chenjing Ding, Haoxuan Dou, Xin Zhang, Weixuan Tang, and Wei Wu. Infinitydrive: Breaking time limits in driving world models. *CoRR*, 2024.
- [36] Mariam Hassan, Sebastian Stapf, Ahmad Rahimi, Pedro M. B. Rezende, Yasaman Haghghi, David Brüggemann, Isinsu Katircioglu, Lin Zhang, Xiaoran Chen, Suman Saha, Marco Cannici, Elie Aljalbout, Botao Ye, Xi Wang, Aram Davtyan, Mathieu Salzmann, Davide Scaramuzza, Marc Pollefeys, Paolo Favaro, and Alexandre Alahi. GEM: A generalizable ego-vision multimodal world model for fine-grained ego-motion, object dynamics, and scene composition control. *CoRR*, 2024.
- [37] Dan Hendrycks and Kevin Gimpel. Gaussian error linear units (gelus). *CoRR*, 2016.
- [38] Martin Heusel, Hubert Ramsauer, Thomas Unterthiner, Bernhard Nessler, and Sepp Hochreiter. Gans trained by a two time-scale update rule converge to a local nash equilibrium. In *NeurIPS*, 2017.
- [39] Irina Higgins, Loic Matthey, Arka Pal, Christopher P Burgess, Xavier Glorot, Matthew M Botvinick, Shakir Mohamed, and Alexander Lerchner. beta-vae: Learning basic visual concepts with a constrained variational framework. In *ICLR*, 2017.
- [40] Jonathan Ho, Ajay Jain, and Pieter Abbeel. Denoising diffusion probabilistic models. In *NeurIPS*, 2020.
- [41] Jonathan Ho, Tim Salimans, Alexey Gritsenko, William Chan, Mohammad Norouzi, and David J Fleet. Video diffusion models. *NeurIPS*, 2022.
- [42] Jordan Hoffmann, Sebastian Borgeaud, Arthur Mensch, Elena Buchatskaya, Trevor Cai, Eliza Rutherford, Diego de Las Casas, Lisa Anne Hendricks, Johannes Welbl, Aidan Clark, Tom Hennigan, Eric Noland, Katie Millican, George van den Driessche, Bogdan Damoc, Aurelia Guy, Simon Osindero, Karen Simonyan, Erich Elsen, Jack W. Rae, Oriol Vinyals, and Laurent Sifre. Training compute-optimal large language models. *CoRR*, 2022.
- [43] Anthony Hu, Gianluca Corrado, Nicolas Griffiths, Zak Murez, Corina Gurau, Hudson Yeo, Alex Kendall, Roberto Cipolla, and Jamie Shotton. Model-based imitation learning for urban driving. In *NeurIPS*, 2022.
- [44] Anthony Hu, Lloyd Russell, Hudson Yeo, Zak Murez, George Fedoseev, Alex Kendall, Jamie Shotton, and Gianluca Corrado. GAIA-1: A generative world model for autonomous driving. *CoRR*, 2023.
- [45] Shengding Hu, Yuge Tu, Xu Han, Chaoqun He, Ganqu Cui, Xiang Long, Zhi Zheng, Yewei Fang, Yuxiang Huang, Weilin Zhao, Xinrong Zhang, Zhen Leng Thai, Kai Zhang, Chongyi Wang, Yuan Yao, Chenyang Zhao, Jie Zhou, Jie Cai, Zhongwu Zhai, Ning Ding, Chao Jia, Guoyang Zeng, Dahai Li, Zhiyuan Liu, and Maosong Sun. Minicpm: Unveiling the potential of small language models with scalable training strategies. *CoRR*, 2024.

- [46] Xiaotao Hu, Wei Yin, Mingkai Jia, Junyuan Deng, Xiaoyang Guo, Qian Zhang, Xiaoxiao Long, and Ping Tan. Drivingworld: Constructing world model for autonomous driving via video GPT. *CoRR*, 2024.
- [47] Yihan Hu, Jiazhi Yang, Li Chen, Keyu Li, Chonghao Sima, Xizhou Zhu, Siqi Chai, Senyao Du, Tianwei Lin, Wenhai Wang, Lewei Lu, Xiaosong Jia, Qiang Liu, Jifeng Dai, Yu Qiao, and Hongyang Li. Planning-oriented autonomous driving. In *CVPR*, 2023.
- [48] Bo Jiang, Shaoyu Chen, Qing Xu, Bencheng Liao, Jiajie Chen, Helong Zhou, Qian Zhang, Wenyu Liu, Chang Huang, and Xinggang Wang. Vad: Vectorized scene representation for efficient autonomous driving. In *ICCV*, 2023.
- [49] Yang Jin, Zhicheng Sun, Ningyuan Li, Kun Xu, Kun Xu, Hao Jiang, Nan Zhuang, Quzhe Huang, Yang Song, Yadong Mu, and Zhouchen Lin. Pyramidal flow matching for efficient video generative modeling. *CoRR*, 2024.
- [50] Bingyi Kang, Yang Yue, Rui Lu, Zhijie Lin, Yang Zhao, Kaixin Wang, Gao Huang, and Jiashi Feng. How far is video generation from world. In *ICLR*, 2025.
- [51] Moo Jin Kim, Karl Pertsch, Siddharth Karamcheti, Ted Xiao, Ashwin Balakrishna, Suraj Nair, Rafael Rafailov, Ethan P Foster, Pannag R Sanketi, Quan Vuong, Thomas Kollar, Benjamin Burchfiel, Russ Tedrake, Dorsa Sadigh, Sergey Levine, Percy Liang, and Chelsea Finn. OpenVLA: An open-source vision-language-action model. In *CoRL*, 2024.
- [52] Diederik P. Kingma and Max Welling. Auto-encoding variational bayes. In *ICLR*, 2014.
- [53] Seungjae Lee, Yibin Wang, Haritheja Etukuru, H. Jin Kim, Nur Muhammad (Mahi) Shafiqullah, and Lerrel Pinto. Behavior generation with latent actions. In *ICML*, 2024.
- [54] Jimmy Lei Ba, Jamie Ryan Kiros, and Geoffrey E Hinton. Layer normalization. In *NeurIPS*, 2016.
- [55] Xiang Li, Yiqun Yao, Xin Jiang, Xuezhi Fang, Xuying Meng, Siqi Fan, Peng Han, Jing Li, Li Du, Bowen Qin, Zheng Zhang, Aixin Sun, and Yequan Wang. Flm-101b: An open llm and how to train it with \$100k budget, 2023.
- [56] Lucas D. Lingle. A large-scale exploration of μ -transfer. *CoRR*, 2024.
- [57] Yaron Lipman, Ricky T. Q. Chen, Heli Ben-Hamu, Maximilian Nickel, and Matthew Le. Flow matching for generative modeling. In *ICLR*, 2023.
- [58] Haotian Liu, Chunyuan Li, Qingyang Wu, and Yong Jae Lee. Visual instruction tuning. In *NeurIPS*, 2023.
- [59] William Ljungbergh, Adam Tonderski, Joakim Johnander, Holger Caesar, Kalle Åström, Michael Felsberg, and Christoffer Petersson. Neuroncap: Photorealistic closed-loop safety testing for autonomous driving. In *ECCV*, 2024.
- [60] Ilya Loshchilov and Frank Hutter. Decoupled weight decay regularization. In *ICLR*, 2019.
- [61] Jiageng Mao, Yuxi Qian, Hang Zhao, and Yue Wang. Gpt-driver: Learning to drive with GPT. *CoRR*, 2023.
- [62] Fabian Mentzer, David Minnen, Eirikur Agustsson, and Michael Tschannen. Finite scalar quantization: Vq-vae made simple. In *ICLR*, 2024.
- [63] Saman Motamed, Laura Culp, Kevin Swersky, Priyank Jaini, and Robert Geirhos. Do generative video models learn physical principles from watching videos? *CoRR*, 2025.
- [64] Jorge Nocedal. Updating quasi newton matrices with limited storage. *Mathematics of Computation*, 1980.
- [65] Maxime Oquab, Timothée Darcet, Théo Moutakanni, Huy V. Vo, Marc Szafraniec, Vasil Khalidov, Pierre Fernandez, Daniel Haziza, Francisco Massa, Alaaeldin El-Nouby, Mido Assran, Nicolas Ballas, Wojciech Galuba, Russell Howes, Po-Yao Huang, Shang-Wen Li, Ishan Misra, Michael Rabbat, Vasu Sharma, Gabriel Synnaeve, Hu Xu, Hervé Jégou, Julien Mairal, Patrick Labatut, Armand Joulin, and Piotr Bojanowski. Dinov2: Learning robust visual features without supervision. In *TMLR*, 2024.
- [66] Myle Ott, Sergey Edunov, Alexei Baevski, Angela Fan, Sam Gross, Nathan Ng, David Grangier, and Michael Auli. fairseq: A fast, extensible toolkit for sequence modeling. In *NAACL*, 2019.
- [67] Valentinos Pariza, Mohammadreza Salehi, and Yuki Asano. Hummingbird evaluation for vision encoders, 2024.

- [68] Adam Polyak, Amit Zohar, Andrew Brown, Andros Tjandra, Animesh Sinha, Ann Lee, Apoorv Vyas, Bowen Shi, Chih-Yao Ma, Ching-Yao Chuang, et al. Movie gen: A cast of media foundation models. *CoRR*, 2024.
- [69] Alec Radford, Jong Wook Kim, Chris Hallacy, Aditya Ramesh, Gabriel Goh, Sandhini Agarwal, Girish Sastry, Amanda Askell, Pamela Mishkin, Jack Clark, Gretchen Krueger, and Ilya Sutskever. Learning transferable visual models from natural language supervision. In *ICML*, 2021.
- [70] Alec Radford, Jeff Wu, Rewon Child, David Luan, Dario Amodei, and Ilya Sutskever. Language models are unsupervised multitask learners. *OpenAI blog*, 2019.
- [71] Jathushan Rajasegaran, Ilija Radosavovic, Yossi Gandelsman Rahul Ravishankar, Christoph Feichtenhofer, and Jitendra Malik. An empirical study of autoregressive pre-training from videos. *CoRR*, 2024.
- [72] Aditya Ramesh, Mikhail Pavlov, Gabriel Goh, Scott Gray, Chelsea Voss, Alec Radford, Mark Chen, and Ilya Sutskever. Zero-shot text-to-image generation. In *ICML*, 2021.
- [73] Jeff Rasley, Samyam Rajbhandari, Olatunji Ruwase, and Yuxiong He. DeepSpeed: System optimizations enable training deep learning models with over 100 billion parameters. In *SIGKDD*, 2020.
- [74] Katrin Renz, Long Chen, Ana-Maria Marcu, Jan Hünemann, Benoît Hanotte, Alice Kamsund, Jamie Shotton, Elahe Arani, and Oleg Sinavski. Carllava: Vision language models for camera-only closed-loop driving. *CoRR*, 2024.
- [75] Robin Rombach, Andreas Blattmann, Dominik Lorenz, Patrick Esser, and Bjorn Ommer. High-resolution image synthesis with latent diffusion models. In *CVPR*, 2022.
- [76] Masaki Saito, Eiichi Matsumoto, and Shunta Saito. Temporal generative adversarial nets with singular value clipping. In *ICCV*, 2017.
- [77] Younggyo Seo, Kimin Lee, Fangchen Liu, Stephen James, and Pieter Abbeel. Harp: Autoregressive latent video prediction with high-fidelity image generator. In *ICIP*, 2022.
- [78] Hao Sha, Yao Mu, Yuxuan Jiang, Li Chen, Chenfeng Xu, Ping Luo, Shengbo Eben Li, Masayoshi Tomizuka, Wei Zhan, and Mingyu Ding. LanguageMPC: Large language models as decision makers for autonomous driving. *CoRR*, 2023.
- [79] Hao Shao, Yuxuan Hu, Letian Wang, Guanglu Song, Steven L. Waslander, Yu Liu, and Hongsheng Li. Lmdrive: Closed-loop end-to-end driving with large language models. In *CVPR*, 2024.
- [80] Uriel Singer, Adam Polyak, Thomas Hayes, Xi Yin, Jie An, Songyang Zhang, Qiyuan Hu, Harry Yang, Oron Ashual, Oran Gafni, Devi Parikh, Sonal Gupta, and Yaniv Taigman. Make-a-video: Text-to-video generation without text-video data. In *ICLR*, 2023.
- [81] Peize Sun, Yi Jiang, Shoufa Chen, Shilong Zhang, Bingyue Peng, Ping Luo, and Zehuan Yuan. Autoregressive model beats diffusion: Llama for scalable image generation. *CoRR*, 2024.
- [82] Suramya Tomar. Converting video formats with ffmpeg. *Linux Journal*, 2006.
- [83] Hugo Touvron, Thibaut Lavril, Gautier Izacard, Xavier Martinet, Marie-Anne Lachaux, Timothée Lacroix, Baptiste Rozière, Naman Goyal, Eric Hambro, Faisal Azhar, Aurélien Rodriguez, Armand Joulin, Edouard Grave, and Guillaume Lample. Llama: Open and efficient foundation language models. *CoRR*, 2023.
- [84] Hugo Touvron, Louis Martin, Kevin Stone, Peter Albert, Amjad Almahairi, Yasmine Babaei, Nikolay Bashlykov, Soumya Batra, Prajjwal Bhargava, Shruti Bhosale, Dan Bikel, Lukas Blecher, Cristian Canton-Ferrer, Moya Chen, Guillem Cucurull, David Esiobu, Jude Fernandes, Jeremy Fu, Wenyin Fu, Brian Fuller, Cynthia Gao, Vedanuj Goswami, Naman Goyal, Anthony Hartshorn, Saghar Hosseini, Rui Hou, Hakan Inan, Marcin Kardas, Viktor Kerkez, Madian Khabsa, Isabel Kloumann, Artem Korenev, Punit Singh Koura, Marie-Anne Lachaux, Thibaut Lavril, Jenya Lee, Diana Liskovich, Yinghai Lu, Yuning Mao, Xavier Martinet, Todor Mihaylov, Pushkar Mishra, Igor Molybog, Yixin Nie, Andrew Poulton, Jeremy Reizenstein, Rashi Rungta, Kalyan Saladi, Alan Schelten, Ruan Silva, Eric Michael Smith, Ranjan Subramanian, Xiaoqing Ellen Tan, Binh Tang, Ross Taylor, Adina Williams, Jian Xiang Kuan, Puxin Xu, Zheng Yan, Iliyan Zarov, Yuchen Zhang, Angela Fan, Melanie Kambadur, Sharan Narang, Aurélien Rodriguez, Robert Stojnic, Sergey Edunov, and Thomas Scialom. Llama 2: Open foundation and fine-tuned chat models. *CoRR*, 2023.
- [85] Sergey Tulyakov, Ming-Yu Liu, Xiaodong Yang, and Jan Kautz. Mocogan: Decomposing motion and content for video generation. In *CVPR*, 2018.

- [86] Thomas Unterthiner, Sjoerd van Steenkiste, Karol Kurach, Raphaël Marinier, Marcin Michalski, and Sylvain Gelly. Fvd: A new metric for video generation. In *DGS@ICLR*, 2019.
- [87] Dani Valevski, Yaniv Leviathan, Moab Arar, and Shlomi Fruchter. Diffusion models are real-time game engines, 2024.
- [88] Aaron Van Den Oord, Oriol Vinyals, et al. Neural discrete representation learning. In *NeurIPS*, 2017.
- [89] Veo-Team, :, Agrim Gupta, Ali Razavi, Andeep Toor, Ankush Gupta, Dumitru Erhan, Eleni Shaw, Eric Lau, Frank Belletti, Gabe Barth-Maron, Gregory Shaw, Hakan Erdogan, Hakim Sidahmed, Henna Nandwani, Hernan Moraldo, Hyunjik Kim, Irina Blok, Jeff Donahue, José Lezama, Kory Mathewson, Kurtis David, Matthieu Kim Lorrain, Marc van Zee, Medhini Narasimhan, Miaosen Wang, Mohammad Babaeizadeh, Nelly Papalampidi, Nick Pezzotti, Nilpa Jha, Parker Barnes, Pieter-Jan Kindermans, Rachel Hornung, Ruben Villegas, Ryan Poplin, Salah Zaiem, Sander Dieleman, Sayna Ebrahimi, Scott Wisdom, Serena Zhang, Shlomi Fruchter, Signe Nørly, Weizhe Hua, Xinchun Yan, Yuqing Du, and Yutian Chen. *Veo 2. tech report*, 2024.
- [90] Ruben Villegas, Mohammad Babaeizadeh, Pieter-Jan Kindermans, Hernan Moraldo, Han Zhang, Mohammad Taghi Saffar, Santiago Castro, Julius Kunze, and Dumitru Erhan. Phenaki: Variable length video generation from open domain textual descriptions. In *ICLR*, 2023.
- [91] Pauli Virtanen, Ralf Gommers, Travis E. Oliphant, Matt Haberland, Tyler Reddy, David Cournapeau, Evgeni Burovski, Pearu Peterson, Warren Weckesser, Jonathan Bright, Stéfan J. van der Walt, Matthew Brett, Joshua Wilson, K. Jarrod Millman, Nikolay Mayorov, Andrew R. J. Nelson, Eric Jones, Robert Kern, Eric Larson, C J Carey, İlhan Polat, Yu Feng, Eric W. Moore, Jake VanderPlas, Denis Laxalde, Josef Perktold, Robert Cimrman, Ian Henriksen, E. A. Quintero, Charles R. Harris, Anne M. Archibald, Antônio H. Ribeiro, Fabian Pedregosa, Paul van Mulbregt, and SciPy 1.0 Contributors. SciPy 1.0: Fundamental Algorithms for Scientific Computing in Python. *Nature Methods*, 2020.
- [92] A Waswani, N Shazeer, N Parmar, J Uszkoreit, L Jones, A Gomez, L Kaiser, and I Polosukhin. Attention is all you need. In *NeurIPS*, 2017.
- [93] Zhenhua Xu, Yujia Zhang, Enze Xie, Zhen Zhao, Yong Guo, Kwan-Yee K. Wong, Zhenguo Li, and Hengshuang Zhao. Drivegpt4: Interpretable end-to-end autonomous driving via large language model. *IEEE RAL*, 2024.
- [94] Wilson Yan, Yunzhi Zhang, Pieter Abbeel, and Aravind Srinivas. Videogpt: Video generation using vq-vae and transformers. *CoRR*, 2021.
- [95] Greg Yang, Edward J. Hu, Igor Babuschkin, Szymon Sidor, Xiaodong Liu, David Farhi, Nick Ryder, Jakub Pachocki, Weizhu Chen, and Jianfeng Gao. Tensor programs V: tuning large neural networks via zero-shot hyperparameter transfer. *CoRR*, 2022.
- [96] Jiazhi Yang, Shenyan Gao, Yihang Qiu, Li Chen, Tianyu Li, Bo Dai, Kashyap Chitta, Penghao Wu, Jia Zeng, Ping Luo, Jun Zhang, Andreas Geiger, Yu Qiao, and Hongyang Li. Generalized predictive model for autonomous driving. In *CVPR*, 2024.
- [97] Yiqun Yao, Siqi fan, Xiusheng Huang, Xuezhi Fang, Xiang Li, Ziyi Ni, Xin Jiang, Xuying Meng, Peng Han, Shuo Shang, Kang Liu, Aixin Sun, and Yequan Wang. nanolm: an affordable llm pre-training benchmark via accurate loss prediction across scales, 2023.
- [98] Lijun Yu, Yong Cheng, Kihyuk Sohn, José Lezama, Han Zhang, Huiwen Chang, Alexander G. Hauptmann, Ming-Hsuan Yang, Yuan Hao, Irfan Essa, and Lu Jiang. Magvit: Masked generative video transformer. In *CVPR*, 2023.
- [99] Lijun Yu, Jose Lezama, Nitesh Bharadwaj Gundavarapu, Luca Versari, Kihyuk Sohn, David Minnen, Yong Cheng, Agrim Gupta, Xiuye Gu, Alexander G Hauptmann, Boqing Gong, Ming-Hsuan Yang, Irfan Essa, David A Ross, and Lu Jiang. Language model beats diffusion - tokenizer is key to visual generation. In *ICLR*, 2024.
- [100] Jiang-Tian Zhai, Ze Feng, Jihao Du, Yongqiang Mao, Jiang-Jiang Liu, Zichang Tan, Yifu Zhang, Xiaoqing Ye, and Jingdong Wang. Rethinking the open-loop evaluation of end-to-end autonomous driving in nusenes. *CoRR*, 2023.
- [101] Xiaohua Zhai, Basil Mustafa, Alexander Kolesnikov, and Lucas Bayer. Sigmoid loss for language image pre-training. In *ICCV*, 2023.
- [102] Richard Zhang, Phillip Isola, Alexei A. Efros, Eli Shechtman, and Oliver Wang. The unreasonable effectiveness of deep features as a perceptual metric. In *CVPR*, 2018.

- [103] Ciyou Zhu, Richard H. Byrd, Peihuang Lu, and Jorge Nocedal. Algorithm 778: L-bfgs-b: Fortran subroutines for large-scale bound-constrained optimization. *ACM Trans. Math. Softw.*, 1997.
- [104] Zheng Zhu, Xiaofeng Wang, Wangbo Zhao, Chen Min, Nianchen Deng, Min Dou, Yuqi Wang, Botian Shi, Kai Wang, Chi Zhang, Yang You, Zhaoxiang Zhang, Dawei Zhao, Liang Xiao, Jian Zhao, Jiwen Lu, and Guan Huang. Is sora a world simulator? a comprehensive survey on general world models and beyond, 2024.
- [105] Brianna Zitkovich, Tianhe Yu, Sichun Xu, Peng Xu, Ted Xiao, Fei Xia, Jialin Wu, Paul Wohlhart, Stefan Welker, Ayzaan Wahid, Quan Vuong, Vincent Vanhoucke, Huong Tran, Radu Soricut, Anikait Singh, Jaspiar Singh, Pierre Sermanet, Pannag R Sanketi, Grecia Salazar, Michael S Ryoo, Krista Reymann, Kanishka Rao, Karl Pertsch, Igor Mordatch, Henryk Michalewski, Yao Lu, Sergey Levine, Lisa Lee, Tsang-Wei Edward Lee, Isabel Leal, Yuheng Kuang, Dmitry Kalashnikov, Ryan Julian, Nikhil J Joshi, Alex Irpan, brian ichter, Jasmine Hsu, Alexander Herzog, Karol Hausman, Keerthana Gopalakrishnan, Chuyuan Fu, Pete Florence, Chelsea Finn, Kumar Avinava Dubey, Danny Driess, Tianli Ding, Krzysztof Marcin Choromanski, Xi Chen, Yevgen Chebotar, Justice Carbajal, Noah Brown, Anthony Brohan, Montserrat Gonzalez Arenas, and Kehang Han. RT-2: Vision-language-action models transfer web knowledge to robotic control. In *CoRL*, 2023.